ARTICLE IN PRESS

Catalysis Today xxx (xxxx) xxx

Contents lists available at ScienceDirect

Catalysis Today

journal homepage: www.elsevier.com/locate/cattod

N-doped activated carbon as support of Pd-Sn bimetallic catalysts for nitrate catalytic reduction

I. Sanchis *, J.J. Rodriguez, A.F. Mohedano, E. Diaz

Department of Chemical Engineering, Universidad Autónoma de Madrid, Crta Colmenar Viejo km 15, 28049 Madrid, Spain

ARTICLE INFO

Keywords:
Hydrothermal carbonization
Lignocellulosic wastes
Waste valorization
N-doping
Denitrification

ABSTRACT

This work studies the catalytic reduction of nitrate using N-doped activated carbon catalysts. Activated carbons were prepared by hydrothermal carbonization (220 °C, 80 % water, 16 h) of garden and park waste and olive stones using $(NH_4)_2SO_4$ as N source, followed by chemical activation with H_3PO_4 at 500 °C (N_2 atmosphere, 1 h). These were impregnated with Pd and Sn to prepare bimetallic catalysts for nitrate catalytic reduction. N-doping improved the BET surface area up to 1369 $m^2\ g^{-1}$ and increased the N content on the catalyst surface to 3 wt%. The N-doped catalysts showed better catalytic performance than the non-doped ones, showing high stability for 100 h on stream, reaching even higher activity than a catalyst supported on a commercial activated carbon. N-doping also showed a positive effect by decreasing NH_4^+ selectivity. Finally, natural and drinking waters spiked with NO_3^- were treated in continuous flow, exhibiting the N-doped activated carbon catalysts, prepared from garden and park waste, a high tolerance to ions other than NO_3^- present in the water solution.

1. Introduction

Waste management is one of the biggest environmental and social problems in the world, mainly due to the increasing population and the linear economy on which today's society is based on [1]. Biomass sources, including wood wastes, agricultural crops and their waste products, municipal and animal wastes, can be considered potential sources of fuel and chemical feedstocks [2–5]. The use of biomass residues as activated carbon precursors also represents an alternative for the management of biomass wastes [6]. Among thermochemical processes to transform these wastes into value products, hydrothermal carbonization (HTC) emerges as an interesting option [7–9].

HTC is a thermochemical process that causes a decrease in the oxygen and hydrogen content of the feedstock through mainly dehydration and decarboxylation reactions [10–12]. This technique is widely used to convert biomass wastes into a solid fraction, called hydrochar, which present improved physicochemical characteristics than feedstock [13]. HTC temperature ranges within 180–250 °C [6,14,15] with residence times between 5 min and 24 h [7–9,15–17]. Raw materials such as lignocellulosic [15,18–20], agricultural [11,21–23], livestock [24–26], domestic waste [27–29] and sewage sludge [30–32] have been used to produce hydrochars with potential applications in agricultural, medicinal, environmental and energy fields [33–35].

HTC serves as a biomass pre-treatment to obtain and stable char, prior to subsequent physical [36–39] or chemical activation [40–42]. Chemical activation has been widely used to prepare activated carbons from hydrochar of biomass wastes. Zubbri et al. [43] prepared an activated carbon from a hydrochar of rambutan peels (170 °C, 90 min, pH 3.6, $A_{BET} = 12.3\ m^2\ g^{-1}$) by chemical activation with KOH (2:1 KOH:HC w/w, 850 °C, 2 h) obtaining an activated carbon with a surface area of 1487 $m^2\ g^{-1}$ and micropore volume of 0.61 $cm^3\ g^{-1}$ (72.7 % of total pore volume). Tu et al. [44] used sewage sludge as hydrochar precursor (200 °C, 5 h, $A_{BET} = 22.2\ m^2\ g^{-1}$) to obtain an activated carbon with a surface area of 1466 $m^2\ g^{-1}$ after KOH activation (2.5 M, 500 °C, 30 min). Diaz et al. [11] used several reagents (KOH, $FeCl_3$, H_3PO_4) to activate a hydrochar from grape seeds (220 °C, 16 h, 60 % humidity). They reported enhanced mesoporosity development ($V_{meso} = 0.23\ cm^3\ g^{-1}$) using H_3PO_4 (3:1 H_3PO_4:HC w/w, 500 °C, 2 h) and increased microporosity ($V_{micro} = 0.98\ cm^3\ g^{-1}$) and high BET surface area ($A_{BET} = 2194\ m^2\ g^{-1}$) using KOH (3:1 KOH:HC w/w, 750 °C, 1 h).

Recently, N-doping of carbon materials has attracted attention. The N doped in the carbon skeleton change the charge density distribution and bond length of the carbon atoms near the dopants. The higher electronegativity of N (3.04) than that of C (2.55) leads electron transfer from the C to the N atom and generates the positive in the C atom adjacent to the N dopant, favoring the electrochemical activity of the

* Corresponding author.
E-mail address: ines.sanchis@uam.es (I. Sanchis).

https://doi.org/10.1016/j.cattod.2023.01.018
Received 31 October 2022; Received in revised form 28 December 2022; Accepted 22 January 2023
Available online 24 January 2023

material [45–47]. N-doped carbons have been used in several applications as energy storage [48–50], pollutant adsorption [51–53] or catalysis [54–56]. As metal particles support, Li et al. [57] observed a good adsorption of Pt on N-doped carbon nanotubes because of the activation of carbon atoms neighboring N due to the large electron affinity of nitrogen, favoring the metal dispersion on the carbon surface. Some interest has been shown in the use of N-doped carbon as support for metal catalysts because of their better performance associated with several factors [58]: (i) the introduction of a heteroatom into carbon material allows controlling the size of the supported metal particles and obtaining a narrower particle size distribution; (ii) the use of a higher conductivity support leads to improved chemical reactivity for electron transfer processes in catalytic systems; (iii) the introduction of basic N atoms (pyridinic and pyrrolic N groups) changes the acid-base properties of the support surface [59].

Promising results have been reported using N-doped catalysts. Baeza et al. [60] prepared a N-doped carbon by co-pyrolysis of low-density polyethylene and 1,1-phenanthroline as carbon and nitrogen sources, respectively. This material was used as a support of a Pd catalyst for 4-chlorophenol hydrodechlorination. The results showed a high enhancement of the catalyst activity, from 0.4 mmol g_{Pd}^{-1} min^{-1} with the non-doped support to 55.6 mmol g_{Pd}^{-1} min^{-1} with N-doped catalyst. You et al. [61] doped a wood-based activated carbon with nitric acid by hydrothermal treatment for NO catalytic oxidation. The N-doping improved NO conversion from 30.6 % with the original activated carbon to 56.6 % after the HNO_3 treatment, because of the alteration of pore size and the increase of the surface basicity due to the introduction of N species on carbon surface, including pyrrolic, pyridinic and graphitic nitrogen.

Nitrate (NO_3^-) is one of the most widespread groundwater contaminants in the world, exceeding in many cases the limit values recommended by the World Health Organization (WHO) and other national and supranational regulations. The nitrate presence in water bodies is caused by the discharge of poorly treated industrial and urban wastewater, the deposition of livestock manure and the abusive use of nitrogen fertilizers in the intensive agriculture [62–66]. Nitrate discharges in water are associated to eutrophication and human health problems [67–72], which leads to the need of establishing concentration limits in drinking waters. The European Union [73] establishes maximum concentrations of 50, 0.1 and 0.5 mg L^{-1} for NO_3^-, NO_2^- and NH_4^+, respectively. The WHO recommends a NO_3^- concentration below 10 mg L^{-1} N-NO_3^- (44 mg L^{-1} NO_3^-). Among the treatments currently available to remove NO_3^- from water, two groups of NO_3^- fate techniques can be distinguished, which can be classified as non-destructive and destructive treatments [66]. The first group includes ion exchange, reverse osmosis and electrodialysis, which produce a rejection with a high concentration of NO_3^-. On the other hand, destructive treatments (biological denitrification and catalytic reduction) are aimed to convert NO_3^- into harmless nitrogen gas (N_2) [62,65,74].

Catalytic reduction of NO_3^-, first studied by Vorlop and Tacke [75] is based on the transformation of NO_3^- and NO_2^- to N_2, operating at mild conditions (ambient temperature and pressure) using hydrogen in low amount as reactant, as well as a buffering agent to control the pH [62,64,65,74]. In general, bimetallic catalysts are more effective for nitrate reduction than monometallic ones [76–78]. The formation of undesirable NH_4^+ together with catalyst deactivation in real waters are the main drawbacks hindering the application of catalytic reduction of nitrate [64–66,79–81]. Therefore, the efforts of the scientific community are focused on the development of new catalysts exhibiting high N_2 selectivity and proven stability.

Bimetallic catalysts consist of a noble metal, Pd being the most widely used, and a promoter metal, most commonly Cu, Sn or In [64–66]. Bimetallic Pd-Sn catalysts have shown good activity and selectivity to N_2 as well as high long-term stability [82–85]. The most commonly used materials as support of this active phases have been metal oxides such as Al_2O_3, TiO_2 or SiO_2 [66,78,81,84] and only a few studies have used carbonaceous materials such as activated carbon [86], activated carbon fibers [87], and one prepared by H_3PO_4 activation of grape seeds [88]. Although activated carbon has not been one of the most studied supports, a good stability in terms of metal loss by leaching has been shown compared to Al_2O_3 [89].

The aim of this work is the valorization of lignocellulosic wastes (garden and park waste and olive stones) through the preparation of catalytic supports. Plain and N-doped activated carbons have been synthesized by HTC followed by a chemical activation process using H_3PO_4 as activating agent. The resulting materials were impregnated with Pd and Sn to synthesize bimetallic catalysts for catalytic reduction of nitrate. Bimetallic catalysts have been extensively characterized and tested in continuous flow in the treatment of synthetic and natural waters.

2. Experimental

2.1. Preparation and characterization of supports

Garden and park waste (GPW) and olive stones (OS) were used as raw materials to prepare carbon supports by HTC. The GPW was collected from the Migas Calientes Composting Plant, located in Madrid (Spain), and the OS were provided by Villanueva del Arzobispo Cooperative (Jaén, Spain). The ground feedstock (< 3 mm) was stored in closed containers at room temperature until the HTC experiments were performed.

Raw material (15 g) was carbonized at 220 °C using 80 wt% water in a Teflon-lined stainless-steel vessel (100 mL) under autogenous pressure for 16 h in a muffle furnace (Hobersal serie 8B Mod 12 PR/400, Hobersal, Barcelona, Spain) [53]. The hydrochar was recovered by filtration, washed with deionized water and oven-dried at 105 °C for 24 h (Nabertherm R 60/750/12-C6, Nabertherm, Bremen, Germany). N doping was carried out using $(NH_4)_2SO_4$ (SigmaAldrich, 99 %), which was dissolved into the water fed to the reactor. A C/N mass ratio of 5 was used [90].

Activated carbons (AC) were prepared by chemical activation using phosphoric acid (H_3PO_4) [11], which was physically mixed with ground hydrochar at H_3PO_4:HC mass ratio of 3:1. The mixture was heated at 500 °C for 1 h under a continuous N_2 flow of 100 N mL min^{-1}. The activation temperature was reached at a heating rate of 10 °C min^{-1}. After cooling under nitrogen flow, the resulting activated carbon was washed with deionized water to neutral pH, recovered by filtration, and dried at 105 °C overnight. A commercial activated carbon (CAC) (Merck) was used as a control support. The supports were denoted by indicating the raw material, olive stones (OS) and garden and park waste (GPW), for instance AC-OS or AC-GPW. In the case of N-doped carbons, N was added to the abbreviation (HC_N or AC_N).

The C, H, N and S content was determined by elemental analysis with a LECO CHNS-932 analyser. The porous structure was determined from N_2 adsorption-desorption isotherms at 77 K using a Micromeritics Tristar 3020 automated volumetric gas adsorption equipment. Samples were previously outgassed at 150 °C for 20 h using a Micromeritics VacPrep 061 vacuum degassing system. The ash content was determined in a muffle furnace (Hobersal serie 8B Mod 12 PR/400, Hobersal, Barcelona, Spain) after pyrolyzing the material at 900 °C for 16 h according to ASTM method D3174-11. Hemicellulose, cellulose, and lignin were determined following UNE-EN ISO 16472 and 13906:2008. Temperature programmed desorption (TPD) was used to evaluate the amount of oxygen surface groups. Samples (0.1 g) were heated up to 900 °C at 10 °C min^{-1} in a vertical quartz tube under a continuous N_2 flow of 1 NL min^{-1}. The amounts of evolved CO_2 and CO were analyzed by non-dispersive infrared absorption in a Siemens model Ultramat 22 equipment (Siemens Aktiengesellscho, Munich, Germany). The materials were analyzed by inductively coupled optical emission spectroscopy (Thermo Fisher Scientific IRIS INTREPID II XDL) to determine the concentration of the inorganic elements.

2.2. Preparation and characterization of bimetallic catalysts

Pd-Sn catalysts were prepared by sequential impregnation with 1.5 wt% of Pd and 1 wt% of Sn. Pd impregnation was performed with Na_2PdCl_4 (Sigma Aldrich, 99.99 %) solution in deionized water by incipient wetness. Impregnated materials were dried overnight at 60 °C and calcined at 200 °C for 3 h. The calcination temperature was reached at 3 °C min^{-1} heating rate. Subsequently, Sn impregnation was carried out with $SnCl_2$ (Sigma Aldrich, 99.99 %) in methanol (Scharlau, 99.9 %). Materials were dried and calcined under the same above conditions. Prior to reaction, the catalyst was reduced under H_2 flow (25 N mL min^{-1}) at 100 °C for 1 h, outgassing with N_2. Catalysts were characterized in terms of metal content by a Total Reflection X-ray Fluorescence (TXRF S2 PicoFox, Bruker spectrometer). The pH_{slurry} was determined measuring the pH (pH-meter, Crison) of an aqueous suspension of the sample (1 g) in deionized water (10 mL) after being under stirring overnight [91]. X-ray photoelectron spectra (XPS) were obtained with a Physical Electronics 5700C Multitechnique instrument using MgKa radiation (1253.6 eV). Complimentary techniques like scanning electron microscopy (SEM) and energy-dispersive X-ray spectroscopy (EDX) were employed for further microstructural investigations using a field emission SEM machine Hitachi S-3000 N apparatus. Room temperature powder X-ray diffraction (XRD) patterns were obtained with a Bruker D8 Advance A25 diffractometer with a Bragg Brentano configuration and a lineal detector Lynxeye (Bruker).

2.3. Nitrate reduction experiments

A fixed-bed glass tubular reactor with 6 mm inner diameter and 20 cm long was used for the continuous flow experiments. A scheme of the reactor system is included in Fig. S1. A synthetic 100 mg L^{-1} of NO_3^- solution (SW), prepared dissolving $NaNO_3$ (Panreac, 99 %) in deionized water, was fed upward at a constant flow of 0.25 mL min^{-1} with a peristaltic pump (GILSON MINIPULS 3) with a space-time of 5.6 kg_{cat} h mol^{-1} NO_3^-. During the nitrate reduction experiments, CO_2 (100 N mL min^{-1}) was bubbling inside 2 L of NO_3^- stock solution. The initial pH of the solutions was 4. To minimize gas-liquid mass transfer limitations and reduce channeling and dead volume, glass spheres (Ø = 3 mm) were placed below and above the catalyst bed [92]. The catalyst (0.135 g) was sieved to 100–315 μm to reduce internal diffusion limitations [93] and a low H_2 flow rate (0.13 N mL min^{-1}) was used to reduce the H availability on the catalyst surface and decrease the NH_4^+ selectivity [64–66]. In addition, a natural water (NW) and a three different drinking waters (DW1, DW2 and DW3), used in a previous work [81,82], spiked with 70 mg NO_3^- L^{-1} were used as reaction solutions, at 2.2 kg_{cat} h mol^{-1} NO_3^-. Table 1 shows the composition of water solutions. In addition, Pd-Sn bimetallic catalyst supported on Al_2O_3 [82] was used to compare the performance among catalysts.

Table 1
Characteristics of the solutions used in the nitrate reduction experiments. Drinking waters (DW) spiked with 70 mg L^{-1} NO_3^- by the addition of $NaNO_3$.

	NW	DW1	DW2	DW3
pH	7.2	7.8	7.1	8.5
Conductivity (μS cm^{-1})	393	560	162	987
Dry residue 180 °C (mg L^{-1})	314	322	80	586
Suspension solids (mg L^{-1})	2.5	< 0.1	< 0.1	< 0.1
Na^+ (mg L^{-1})	34.2	31.8	29.0	115.4
NH_4^+ (mg L^{-1})	0.3	0.4	0.4	0.4
K^+ (mg L^{-1})	2.4	0.8	0.2	1.3
Ca^{2+} (mg L^{-1})	62.8	62.9	3.9	76.3
Mg^{2+} (mg L^{-1})	7.8	25.9	1.1	16.1
Cl^- (mg L^{-1})	26.6	7.3	< 0.1	169.8
NO_2^- (mg L^{-1})	< 0.01	< 0.01	< 0.01	< 0.01
NO_3^- (mg L^{-1})	69.8	70	70	70
SO_4^{2-} (mg L^{-1})	22.0	22.6	2.6	39.1
HCO_3^- (mg L^{-1})	117.0	255.1	8.9	244.0

The reaction samples were analyzed by Ion Chromatography on a Metrohm 882 Compact IC plus chromatograph. NO_3^-, NO_2^-, Cl^- and SO_4^{2-} anions were determined using a Metrosep A Supp 5 column, with a mobile phase flow of 0.7 mL min^{-1} of Na_2CO_3 (3.2 mM) and $NaHCO_3$ (1.0 mM). For Na^+, NH_4^+, K^+, Ca^{2+} and Mg^{2+} cations, a Metrosep C4 column was used with 0.9 mL min^{-1} of $C_7H_5NO_4$ (0.7 mM) and HNO_3 (1.7 mM) as mobile phase. Conductivity and pH were measured by a conductivity meter (GLP 31, CRISON) and a pHmeter (GLP 21, CRISON), respectively.

3. Results and discussion

3.1. Characterization of the materials

Table 2 shows the characterization of the raw materials, hydrochar and activated carbons. GPW (moisture content 5 wt%) was composed of lignocellulosic materials including wood, bark, leaves, and grass clippings, exhibiting a complex structure. Analysis of the GPW yielded hemicellulose (28 wt%), cellulose (42 wt%), and lignin (19 wt%). Regarding OS (moisture content 18 wt%), the structure component analysis indicated a content of hemicellulose (25 wt%), cellulose (31 wt %), and lignin (22 wt%) [94–97]. Hydrochar yields, calculated as the mass of the hydrochar per unit mass of raw material on a dry basis, were similar between N-doped and non-doped materials, being 76–80 % and 65–68 % for GPW and OS hydrochar, respectively. During the HTC process hydrolysis, dehydration, and decarboxylation reactions are produced, which generate the losing of H and O in the form of H_2O and CO_2, thereby increasing the carbon content in the solid [53,95,98,99]. Non-doped hydrochar from GPW and OS showed an increase in the carbon content (≈ 53 % and 45 %) and a decrease in oxygen (≈ 53 % and 49 %) and hydrogen (≈ 7 % and 13 %) content. In the case of N-doped hydrochars, the modification of the elemental composition is justified by the incorporation of nitrogen. The use of $(NH_4)_2SO_4$ as doping agent also caused an increase of S content in these hydrochars. N-doped and non-doped hydrochars were characterized by low porosity, exhibiting negligible specific surface area, lower than 4 m^2 g^{-1}. The activation with H_3PO_4 gave rise materials with high surface area, characterized by a higher contribution of mesoporosity, characteristic of using H_3PO_4 as activating agent [11,53]. AC-GPW and AC-OS showed similar BET surface areas, 905 and 971 m^2 g^{-1}, respectively, achieving a high development of mesoporosity, especially in the case of AC-GPW. Moreover, the N-doping caused an increase of the BET surface area, which increased to 1369 and 1168 m^2 g^{-1} for AC_N-GPW and AC_N-OS, respectively. In all cases, prepared activated carbons showed higher surface area and mesoporous volume than the commercial activated carbon used as reference. There is some controversy in the literature about the changes produced in the textural properties by N doping. Ayusheev et al. [58] reported an increase from 210 m^2 g^{-1} to 300 m^2 g^{-1} for BET surface area and from 0.47 cm^3 g^{-1} to 0.88 cm^3 g^{-1} for pore volume, with the incorporation of 2 % of N in carbon nanofibers supports. Similar results were observed by Shalagina et al. [100], who observed BET surface areas 1.2–1.8-fold higher, and micropore volume 2.6–5.7-fold higher in N-doped carbon nanofibers in comparison with pure materials. However, Treeweranuwat et al. [101] noted a high increase in the N/C ratio caused a blockage of the micropores, which resulted in a decrease of the BET surface area, with values of 2245, 2020 and 1940 m^2 g^{-1} for a N/C ratio of 0.02, 0.04 and 0.05, respectively.

Hydrochar activation increased the ash content in all cases, mainly due to the remaining inorganic matter derived from the activating agent, especially the P content [11]. Regarding the elemental analysis, a similar trend of decreasing H and N content was observed for the GPW and OS derived materials after the activation process due to the increase in ash content. Surface oxygen groups on carbon materials decomposed upon heating by releasing CO and CO_2 at different temperatures [102,103]. Hydrochars are characterized by a lower oxygen surface groups than raw materials because of hydrolysis of carbohydrates and proteins along

Table 2
Characteristics of the raw materials (GPW and OS), hydrochars (HC and HC_N) and activated carbons (AC and AC_N).

Material	C wt%	H wt%	N wt%	S wt%	O[a] wt%	Ash wt%	A_{BET} m^2 g^{-1}	V_{meso} cm^3 g^{-1}	V_{micro} cm^3 g^{-1}	CO_2 μmol/g	CO μmol/g
GPW	44.9	5.9	1.8	< 0.1	43.6	3.7	-	-	-	2985	2642
HC-GPW	68.8	5.5	1.5	0.1	20.3	3.8	-	-	-	2188	2440
HC_N-GPW	50.2	5.0	7.3	6.4	27.1	4.0	-	-	-	811	1579
AC-GPW	68.7	2.7	0.6	< 0.1	23.2	4.7	905	0.69	0.19	322	1520
AC_N-GPW	43.9	1.5	2.1	0.1	47.1	5.3	1369	0.80	0.52	295	1104
OS	44.5	6.1	0.2	0.2	48.6	0.4	-	-	-	1250	2831
HC-OS	64.6	5.3	0.3	< 0.1	29.4	0.3	-	-	-	1222	2790
HC_N-OS	40.9	4.9	9.6	10.6	33.7	0.3	-	-	-	968	1884
AC-OS	75.2	2.3	0.3	0.1	20.0	2.1	971	0.45	0.23	247	1425
AC_N-OS	54.1	1.6	2.8	0.8	38.2	2.5	1168	0.76	0.40	394	1760
CAC	82.8	1.3	0.5	0.5	10.1	4.8	870	0.18	0.34	361	789

[a] Calculated by difference O = 100 − (C + H + N + S + Ash).

HTC [104]. Moreover, the introduction of N into the carbon structure at positions previously occupied by C tends to decrease the CO_2 and CO concentration of N-doped hydrochars. In addition, the high temperature during the activation process diminished the presence of surface functional groups.

The characterization of the catalysts obtained after the impregnation of the activated carbons is shown in Table 3. The prepared catalysts were characterized by an acidic pH_{slurry} due to the activation with H_3PO_4 [11], exhibiting higher acidity catalysts prepared from non-doped activated carbons. At the pH of the solution, all the catalysts presented negative surface charge, which did not favor the electrostatic interaction with nitrate. Moreover, this negative charge could increase the adsorption of hydrogen on the catalyst surface. The oxygen surface groups, formed in most of the activated carbons, had an acidic character, which enhanced electron-acceptor properties into the carbon surface [105]. On the other hand, N-doping causes changes in the acid-base properties of the support surface due to the introduction of basic N atoms (pyridinic and pyrrolic N groups) [59], inducing electron-donor properties [106]. The impregnation process gave rise to a decrease in pore volume. The most important reduction was exhibited by N-doped catalysts, decreasing the surface area by 27 % and 20 % for Pd-Sn/AC_N-GPW and Pd-Sn/AC_N-OS, respectively. This loss of surface area was originated mainly from mesopores plugging, with a decrease of 29 % and 37 % in the mesopore volume for GPW and OS materials, respectively.

Fig. 1 exhibits the Pd and Sn mapping distribution of the fresh catalysts. These images show clear differences in the morphology of the supports depending on the raw material, because the outer surface of the catalysts showed different sizes and shapes. The GPW derived catalysts presented an irregular structure, in which cracks and crevices could be observed throughout the catalysts surface. In addition, some small pores, around 5–7 μm, originating from the activation process could be observed. However, the OS derived catalysts showed a heterogeneous morphology, with a wide variety of small fragments with different shapes, where no developed porous structure could be differentiated.

Table 3
Characteristics of the Pd-Sn (1.5–1 wt%) catalysts.

Catalyst	pH_{slurry}	Pd_{bulk} wt%	Sn_{bulk} wt%	A_{BET} m^2 g^{-1}	V_{meso} cm^3 g^{-1}	V_{micro} cm^3 g^{-1}
Pd-Sn/AC-GPW	2.3	1.6	1.0	823	0.65	0.18
Pd-Sn/AC_N-GPW	3.8	1.6	1.1	993	0.57	0.39
Pd-Sn/AC-OS	1.9	1.5	1.1	837	0.41	0.15
Pd-Sn/AC_N-OS	3.4	1.6	1.0	930	0.48	0.39
Pd-Sn/CAC	5.0	1.5	1.0	728	0.17	0.30

Table 4 shows the element concentration on the catalysts surface analyzed by XPS. The results confirmed the presence of N on the catalyst surface due to N-doping, while the N content on the surface of non-doped catalysts was negligible before their use in reaction (Table S1). Among N-doped catalysts, Pd-Sn/AC_N-GPW catalyst showed higher N_{XPS} content on the catalyst surface than Pd-Sn/AC_N-OS, being 3.0 and 1.4 wt %, respectively. After nitrate reduction, a slight N accumulation was observed on the catalysts surface, especially in the case of Pd-Sn/AC-GPW. Regarding the metal distribution on the catalysts surface, mapping images describes properly the data reported in Table 4. As can be seen, the distribution of both metals on the catalysts surface was very different depending on the raw material. In the case of GPW-derived catalysts, Fig. 1a and Fig. 1b, the distribution of Pd (Pd_{XPS} = 7.6 and 13.8 wt%, respectively) and Sn (Sn_{XPS} = 10.4 and 16.8 wt%, respectively) was homogeneous on the catalysts surface, being both metals well distributed on the support surface. However, the distribution of the active phase on the OS-derived supports was different. In the case of Pd-Sn/AC-OS catalysts, Fig. 1c, most of the support surface was covered by Sn (Sn_{XPS} = 30.9 wt%), being the Pd (Pd_{XPS} = 7.2 wt%) slightly concentrated in some areas, but mostly forming Pd clusters, represented by bright yellow dots. Regarding Pd-Sn/AC_N-OS catalyst, Fig. 1d, Pd (Pd_{XPS} = 12.6 wt%) was found to be better distributed on the support surface, with various Pd clusters and with a high Sn content on the catalyst surface (Sn_{XPS} = 43.6 wt%). In the case of Pd-Sn/CAC catalyst, Fig. 1e, the block structure without a clearly visible porosity and a broad of shapes and sizes was observed, where both metals (Sn_{XPS} = 20.9 wt%; Pd_{XPS} = 13.7 wt%) were adsorbed on the support surface, with some Pd clusters also appearing.

XPS analysis of the catalysts surface (Table 5 and Fig. 2) shows the relative distribution and the spectra of C1s, O1s and N1s, respectively, including the decomposed peaks. Supporting information includes the relative distribution and the spectra of C1s, O1s and N1s for the used catalysts (Table S2), the specific binding energy for each decomposed peak (Table S3) and the spectra of the used catalysts (Fig. S2). The C1s spectra can be resolved into six individual component peaks [61,107,108], carbidic carbon, graphitic carbon, alcohol or ether groups, carbonyl groups, carboxyl or ester groups and peaks due to π-π* transitions in aromatic rings. As can be seen in the C1s spectra, the prepared catalysts presented only 3 peaks, corresponding to the graphitic carbon, carbon present in form of alcohol and ether groups, and carbonyl groups. The deconvolution of these peaks showed graphitic carbon as the main carbon component on the catalysts surface, with a relative distribution between 67.5 % and 74.8 % in the fresh catalysts. An increase of alcohol and ether groups could be observed in Pd-Sn/AC_N-GPW and Pd-Sn/AC_N-OS catalysts with respect the non-doped materials, which became more evident after their use in the reaction. The deconvolution of O1s spectra of the prepared catalysts revealed the presence of 4 peaks in most of them, being 5 peaks in the case of Pd-Sn/AC-GPW [102,108,109]. The fresh catalysts derived from the olive stones presented a similar distribution, being the average composition:

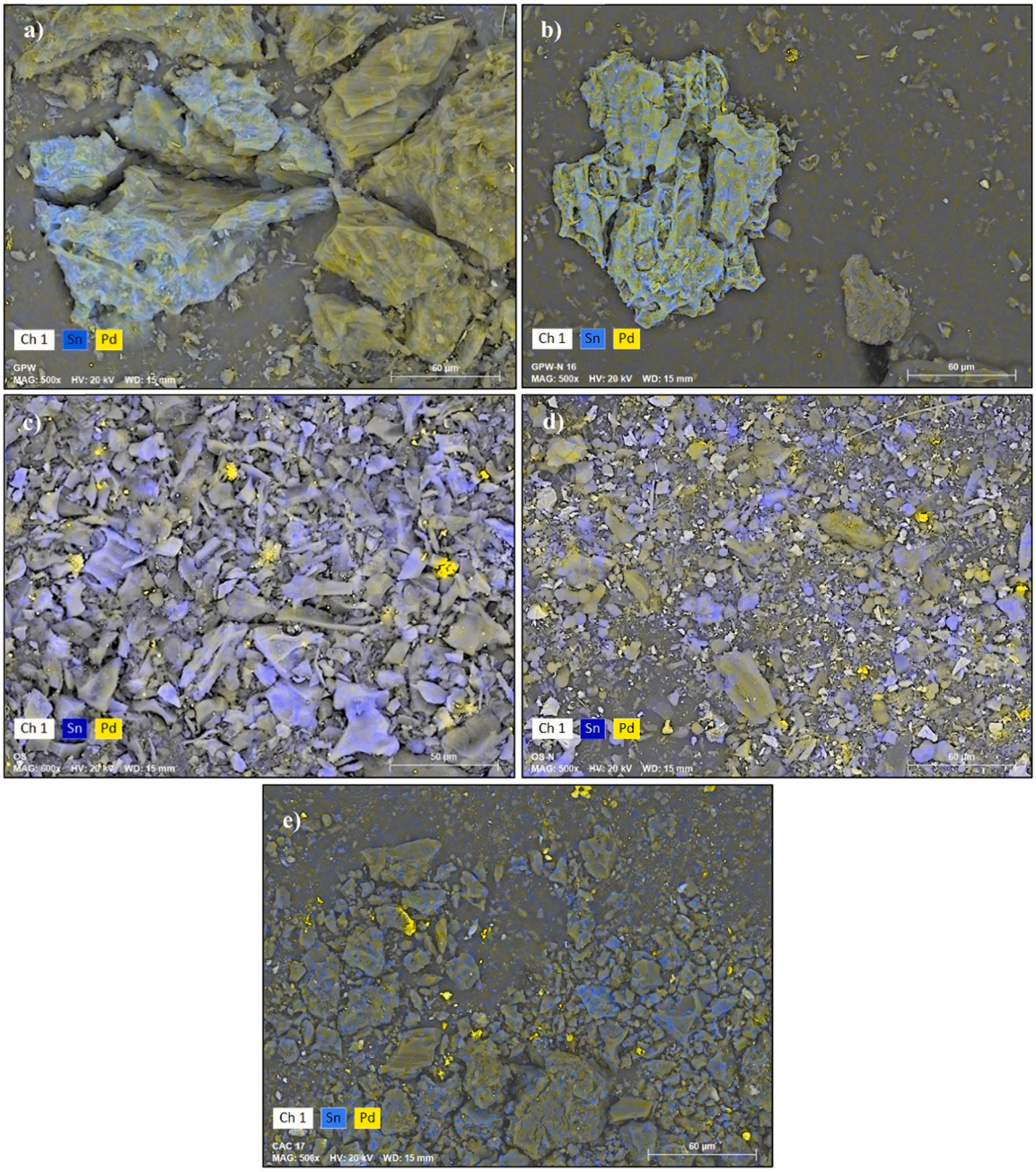

Fig. 1. Energy Dispersive X-ray Spectroscopy (EDX) mapping of Scanning Electron Micrographs (SEM) of Pd (yellow) and Sn (blue) on the catalysts: a) Pd-Sn/AC-GPW, b) Pd-Sn/AC_N-GPW, c) Pd-Sn/AC-OS, d) Pd-Sn/AC_N-OS, and e) Pd-Sn/CAC.

Table 4
Element concentration (atomic/wt%) on the surface of fresh catalysts.

Catalyst	Pd_{XPS} (%)	Sn_{XPS} (%)	C_{XPS} (%)	O_{XPS} (%)	N_{XPS} (%)
Pd-Sn/AC-GPW	1.3/7.6	1.6/10.4	60.0/ 39.6	25.5/ 22.4	-
Pd-Sn/AC_N-GPW	2.3/13.8	2.5/16.8	79.0/ 53.6	10.4/9.4	3.8/3.0
Pd-Sn/AC-OS	1.4/7.2	5.4/30.9	72.5/ 41.9	15.2/ 11.7	-
Pd-Sn/AC_N-OS	3.4/12.6	10.6/ 43.6	55.4/ 23.1	20.8/ 11.5	2.8/1.4
Pd-Sn/CAC	2.4/13.7	3.3/20.9	81.9/ 52.6	10.1/8.6	-

22.1–25.4 % of quinones and carbonyl groups, 36.4–38.4 % of lactones, carboxylic anhydrides, phenol and ether groups, 25.9–31.0 % carboxylic acid, and 10.2–10.5 % chemisorbed water. As can be seen, after their use in the catalytic reduction of nitrate, the oxygen distribution on the surface of the catalysts seemed to be more similar. The N content on the surface of the non-doped fresh catalysts was negligible, so the spectra of the Pd-Sn/AC-GPW, Pd-Sn/AC-OS and Pd-Sn/CAC catalysts are not shown. However, after their use in reaction, the N concentration on the catalysts surface increased, although not enough to form a peak in the case of Pd-Sn/AC-OS and Pd-Sn/CAC catalysts, which presented 0.3 wt% N (Fig. S2). Theoretically, N atoms are promoted to form four configurations of pyridinic-N, pyrrolic-N, graphitic-N, and N-oxides [47, 61,110–112]. The fresh N-doped catalysts presented a similar distribution of the N species on their surface, however, Pd-Sn/AC_N-GPW catalyst showed a slightly higher concentration of pyridinic-N and lower of

Table 5
Relative distribution (%) of C1s, O1s and N1s on the surface of fresh catalysts.

		Pd-Sn/ AC-GPW	Pd-Sn/ AC_N-GPW	Pd-Sn/ AC-OS	Pd-Sn/ AC_N-OS	Pd-Sn/ CAC
C1s	Graphitic-C	74.8	70.2	70.7	67.5	69.2
	Alcohol/ether	16.9	21.7	19.7	23.9	21.8
	Carbonyl	8.3	8.1	9.6	8.6	9.0
O1s	Carbonyl/quinone	11.8	19.1	22.1	25.4	18.0
	Phenol, ether, lactone, carboxylic anhydride	16.6	31.7	36.4	38.4	29.7
	-COOH	25.3	34.3	31.0	25.9	32.8
	Chemisorbed H_2O	34.1	14.9	10.5	10.2	19.4
	CO_2/ CO	12.3	-	-	-	-
N1s	Pyridinic-N	-	33.3	-	29.4	-
	Pyrrolic-N	-	27.1	-	27.2	-
	Graphitic-N	-	27.8	-	33.4	-
	N-oxide species	-	11.8	-	9.9	-

graphitic-N than Pd-Sn/AC_N-OS.

The XRD patterns of the fresh catalysts are shown in Fig. S3. With respect to the active phase, the characteristic diffraction peaks at 40.1°, 46.7° and 68.1° can be attributed to Pd [113,114] and the peak at 34.01° to PdO [115]. The diffractograms also exhibited peaks for Sn at 30.5°, 31.8°, SnO at 29.7°, 56.9° and SnO_2 at 26.5°, 38.1°, 43.0° and 52.5° [116]. The diffractograms of the GPW-derived catalysts showed a wider variety of peaks than OS-derived catalysts, especially in the case of Pd-Sn/AC-OS catalyst, which only appeared the peaks attributed to Pd. In all cases, the XRD patterns of the catalysts showed significant peaks around $2\theta = 25°$ and 44°. These peaks were attributed to the hexagonal graphite structures (002) and (100), respectively [117].

Deconvolution of the core-level spectra of Pd3d and Sn3d orbital evidence the existence of zerovalent and electrodeficient Pd and Sn species. In the case of Pd catalysts, two main bands centered at binding energy values of 335.5 and 337.0 eV were observed for Pd $3d_{5/2}$, which can be attributed to a zerovalent and electrodeficient Pd species, (Pd^0) and (PdO), respectively. The Sn spectra presented three peaks at 485.1, 486.2, and 487.3 eV, corresponding to zerovalent Sn species (Sn^0), and electrodeficient Sn species (SnO, and SnO_2), respectively. Table 6 collects the relative atomic distribution of the reduced and oxidized species of for both metals. The oxidized species were predominating for both metals in all catalysts except for Pd-Sn/AC_N-GPW catalyst, which presented a high concentration of zerovalent Pd in the catalyst surface together with the lowest concentration of Sn^0. This fact could be associated with the high availability of active sites (Pd^0) for initial H_2 activation ($Pd^0 + H_2 \rightarrow$ Pd-$2H_{ads}$) [118,119], and consequently SnO/SnO_2 rejuvenation to Sn^0 by H_{ads} [119].

3.2. Nitrate reduction experiments

Fig. 3 shows the results of NO_3^- conversion and NH_4^+ selectivity for the bimetallic Pd-Sn catalysts supported on CAC, AC-GPW, AC_N-GPW, AC-OS and AC_N-OS. NO_2^- was not detected in the reaction medium. The Pd-Sn/CAC and Pd-Sn/AC_N-GPW catalysts reached equilibrium conversion within the first 5 h on stream, whereas the Pd-Sn/AC-GPW catalyst took around 20 h. The NO_3^- conversion stabilized at 85 %, 60 % and 100 % for Pd-Sn/CAC, Pd-Sn/AC-GPW and Pd-Sn/AC_N-GPW catalysts, respectively. These data revealed a positive effect of N-doping, which not only improved the nitrate conversion with respect to the Pd-Sn/AC-GPW catalyst, but also increased the conversion obtained with

Table 6
Relative distribution (%) of Pd3d and $Sn3d_{5/2}$ on the surface of fresh catalysts.

		Pd-Sn/ AC-GPW	Pd-Sn/ AC_N-GPW	Pd-Sn/ AC-OS	Pd-Sn/ AC_N-OS	Pd-Sn/ CAC
Pd3d	Pd^0	36.9	70.2	38.0	31.1	42.3
	PdO	63.1	29.8	62.0	68.9	57.7
$Sn3d_{5/2}$	Sn^0	31.5	16.4	31.7	32.6	33.5
	SnO	37.3	47.2	37.3	35.3	38.3
	SnO_2	31.2	36.4	31.0	32.1	28.2

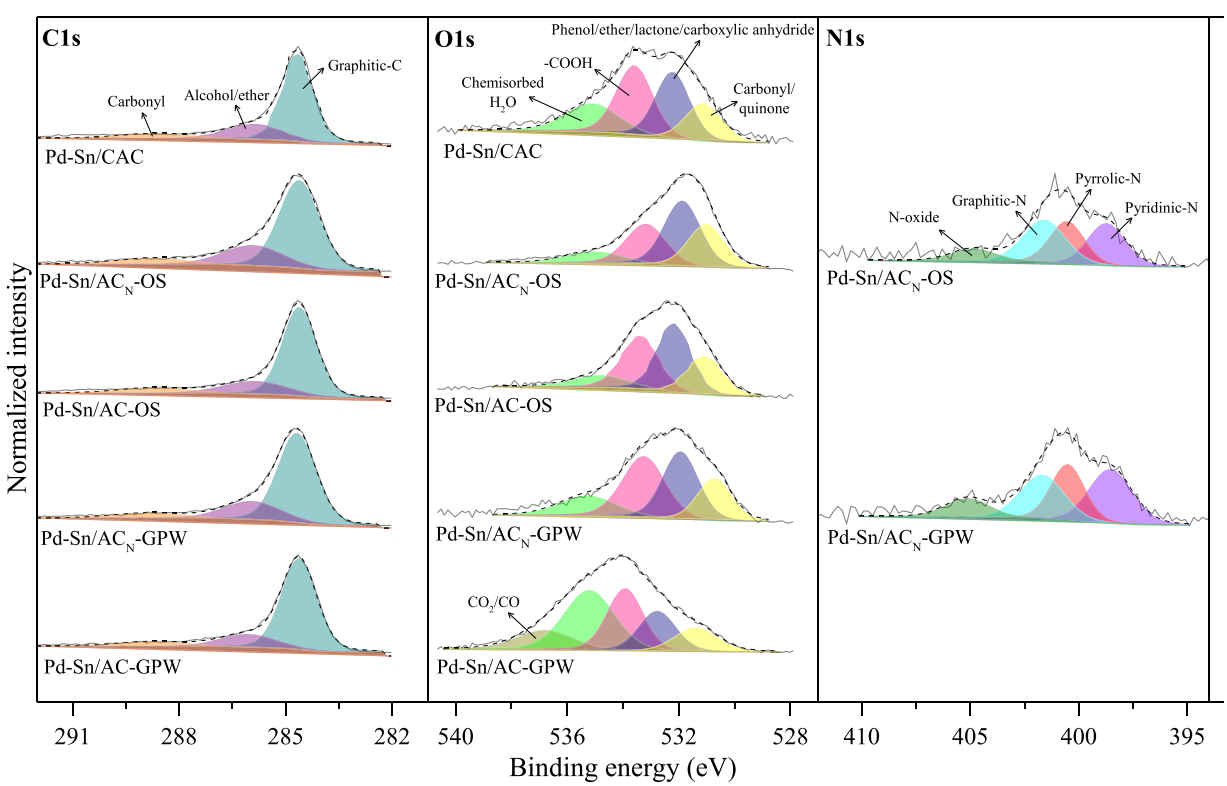

Fig. 2. XPS spectra of C1s, O1s and N1s of the fresh catalysts.

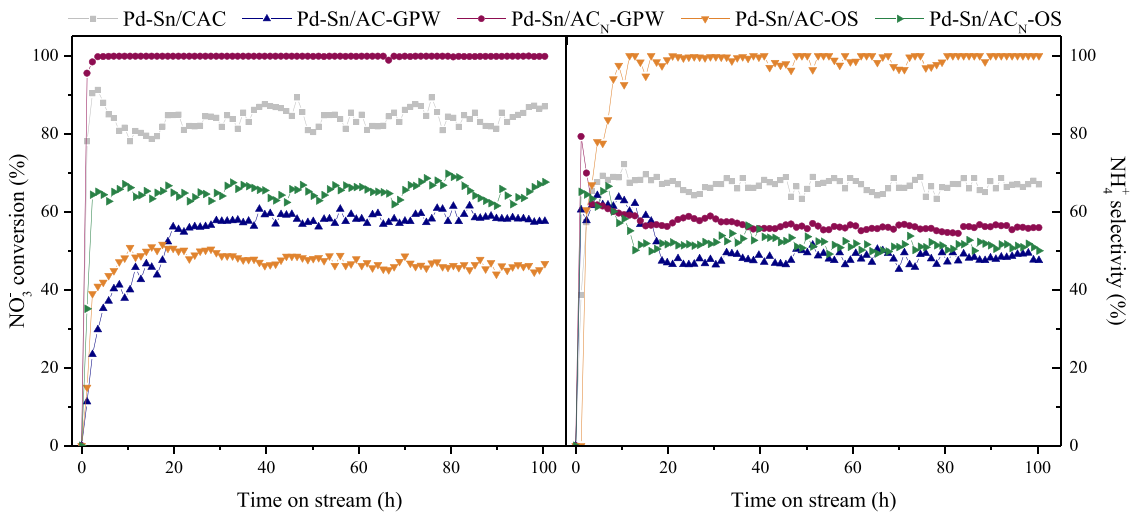

Fig. 3. NO_3^- conversion (%) and NH_4^+ selectivity (%) of Pd-Sn (1.5–1 wt%) catalysts supported on CAC, AC-GPW, AC_N-GPW, AC-OS and AC_N-OS in synthetic water (SW). Space-time of 5.6 kg_{cat} h mol^{-1} NO_3^-.

the catalyst supported on the commercial activated carbon. The Pd-Sn/AC-OS and Pd-Sn/AC_N-OS catalysts reached the equilibrium conversion at 10 and 2 h on stream, respectively. The OS derived catalysts showed lower NO_3^- conversion than the commercial carbon catalyst (47 % and 65 % for non-doped and N-doped catalysts, respectively). Although NH_4^+ production exceeded the established limit of 0.5 mg L^{-1} for human consumption in all cases, being 15.5, 8.5 and 17.3, 13.7 and 9.9 mg NH_4^+ L^{-1} for Pd-Sn/CAC, Pd-Sn/AC-GPW, Pd-Sn/AC_N-GPW, Pd-Sn/AC-OS and Pd-Sn/AC_N-OS catalysts, respectively, the N-doped catalysts showed a positive effect reducing the selectivity to NH_4^+. In the case of GPW-derived catalysts, the Pd-Sn/AC-GPW achieved a selectivity to NH_4^+ only 15.5 % lower than that obtained by the Pd-Sn/AC_N-GPW catalyst, being the conversion of the latter 1.7 times higher. These differences increased with OS-derived catalysts. The Pd-Sn/AC_N-OS showed 38 % higher nitrate conversion than Pd-Sn/AC-OS catalyst and 48 % lower NH_4^+ selectivity. The low performance of Pd-Sn/AC-OS could be related to a poor NO_3^- adsorption on the promoter metal, that caused a decrease of both NO_3^- reduction and N/H ratio on the catalyst surface, which facilitates the combination of N atom with H to form NH_4^+ instead of the recombination of two N atoms. The increase in NH_4^+ selectivity, compared to other commonly used supports as Al_2O_3 or TiO_2 [66], could be related to the high BET surface area and the high adsorption capacity of these carbon-based catalysts. These factors could enhance the adsorption of H on the catalyst surface, increasing the N/H ratio, which hinders the combination of two atoms of N to form N_2, being NH_4^+ the main reaction by-product.

The good performance showed by the Pd-Sn/AC_N-GPW catalyst could be attributed to the positive effect of the high N content on the catalyst surface (3.0 wt%), more than double the content showed by the Pd-Sn/AC_N-OS catalyst. In addition, the higher electronegativity of N than C leads to the electron transfer from the C atom to the N atom and generate the positive one on the C atom adjacent to the N dopant [45, 46]. This effect could enhance the attraction generated by the catalyst surface to NO_3^- ions, improving the catalyst performance. On the other hand, an increase of pyridinic N on the catalyst surface can increase electron transfer, which enhances the catalytic activity of the materials [47,120]. The XPS results, as mentioned above, revealed that Pd-Sn/AC_N-GPW catalyst presented the highest presence of pyridinic N (33.3 wt%). In addition, as can be seen in the SEM/EDX images (Fig. 1), the GPW-derived catalysts presented a better active phase distribution, without presence of Pd clusters, which could decrease the active surface of the Pd for the H_2 activation, hindering the redox cycle between NO_3^-, Sn and Pd [66].

The Pd-Sn/AC_N-GPW catalyst was selected because of its good performance for the experiments with drinking and natural waters. This catalyst achieved a complete conversion during the experiments above-mentioned at 5.6 kg_{cat} h mol^{-1}. Therefore, following experiments were carried out at 2.2 kg_{cat} h mol^{-1}, more adverse conditions for the catalyst, which allowed to observe differences between nitrate reduction tests, matching the NO_3^- initial concentration of all solutions to the nitrate content in natural water (70 mg L^{-1}). Fig. 4 shows the NO_3^- conversion and NH_4^+ selectivity obtained with the Pd-Sn/AC_N-GPW catalyst in the treatment of synthetic water (SW), natural water (NW) and drinking water (DW). In addition, results obtained with a Pd-Sn/Al_2O_3 catalyst with the same metal content are shown to compare the activated carbon-based catalyst with a widely used support, studied in previous works [81,82]. As can be seen, Pd-Sn/AC_N-GPW reached equilibrium conversion in the first 5 h on stream in the case of SW, while in waters containing ions other than NO_3^-, this time increased to values of 9, 20, 24 and 25 h for DW2, DW3, DW1 and NW, respectively. Decreasing the space-time from 5.6 to 2.2 kg_{cat} h mol^{-1} resulted in Pd-Sn/AC_N-GPW catalyst achieved a 75 % nitrate conversion with synthetic water. The follow higher nitrate conversion, around 62 %, was achieved with DW2 water, which showed the lowest conductivity (162 μS cm^{-1}). The performance of the catalyst in the treatment of DW1 and NW waters was very similar in terms on nitrate conversion (around 50 %), since both showed similar characteristics, with mild conductivities of 560 and 393 μS cm^{-1}, respectively. The catalyst achieved the lowest conversion in DW3 water treatment, around 32 %, due to its high conductivity (987 μS cm^{-1}). These results did not follow the trend observed in previous works using Pd-Sn catalysts supported on alumina [81,82], where in DW1 and DW3 waters, with a high HCO_3^- concentration (255.1 and 244.0 mg L^{-1}, respectively), the presence of higher Cl^- content (169.8 for DW3 versus 7.3 mg L^{-1} for DW1) decreased the negative impact of HCO_3^- on the catalytic activity. However, this fact did not seem to occur in the case of using activated carbon as catalyst support. On the other hand, even using higher space times with the alumina (13.8 kg_{cat} h mol^{-1}) than with activated carbon (2.2 kg_{cat} h mol^{-1}), the Pd-Sn/Al_2O_3 catalyst showed a continuous decrease in nitrate conversion due to catalyst deactivation. However, the Pd-Sn/AC_N-GPW catalyst showed a high stability up to 100 h on stream and a higher tolerance to the presence of ions other than NO_3^- in solution, which may be due to its abundance of surface functional groups and high surface area. Therefore, the carbon surface presents a greater number of adsorption sites for the retention of these ions. In the case of the alumina-supported catalyst, ions such as HCO_3^- or Cl^- can only be adsorbed on the metal active sites, interfering the NO_3^- adsorption and thus its reduction [121, 122]. The selectivity to NH_4^+ can be related to the nitrate conversion, so

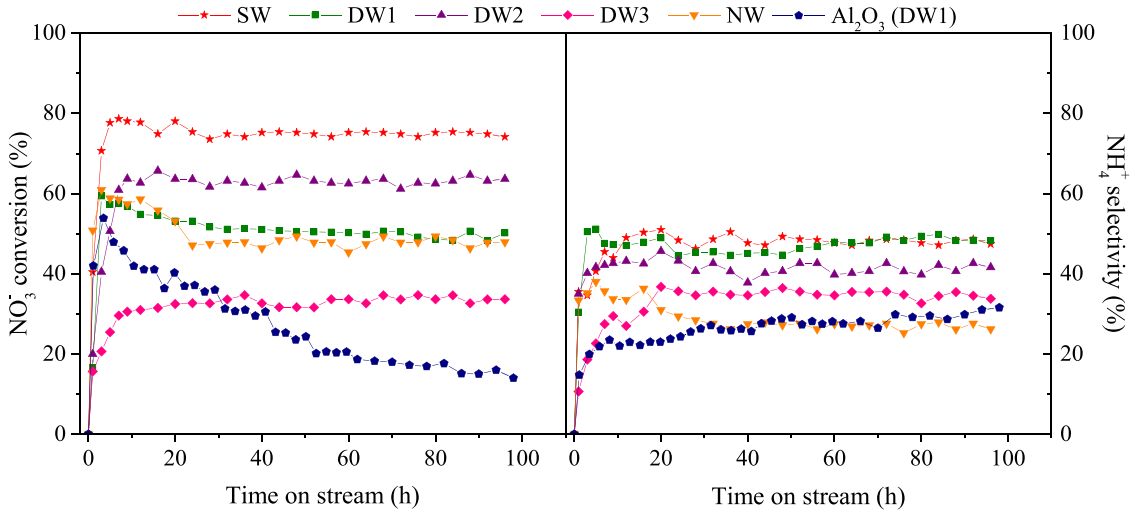

Fig. 4. NO_3^- conversion (%) and NH_4^+ selectivity (%) of Pd-Sn/AC_N-GPW (1.5–1 wt%) catalyst in synthetic water (SW), natural water (NW) and drinking waters (DW1, DW2 and DW3) at space-time of 2.2 kg_{cat} h mol^{-1} NO_3^-. The results obtained for DW1 with the Pd-Sn/Al_2O_3 (1.5–1 wt%) catalyst at 13.8 kg_{cat} h mol^{-1} are included.

increased in the water treatment following the pattern SW > DW2 > DW3. However, the difference showed in the treatment of DW1 and NW waters stand outs, with almost identical nitrate conversion, which can be explain by the modification of the N/H ratio on the catalyst surface by the presence of a higher content of HCO_3^- in the case of DW1 (255.1 mg L^{-1} versus 177.0 mg L^{-1} for NW). The HCO_3^- ion has a similar structure than NO_3^- and can compete for the active sites on the catalyst surface, so the N content on this catalyst surface is reduced, decreasing the N/H ratio, which is related to higher NH_4^+ production [81,82,123,124].

4. Conclusion

The work shows the valorization of garden and park wastes and olive stones by hydrothermal treatment and H_3PO_4 activation for the preparation of Pd-Sn catalysts used in the catalytic reduction of nitrate. The activation process allowed to increase the specific surface area of the hydrochar, achieving activated carbons characterized by a high mesoporosity. N-doping during HTC increased the N content on the catalysts surface, achieving an improvement of their textural properties. The catalysts prepared by the sequential Pd-Sn impregnation on activated carbons achieved high stability in the catalytic reduction of nitrate. N-doped catalysts showed higher nitrate conversion than non-doped catalysts, even better performance than a commercial carbon-based catalyst. Factors such as the N content on the catalyst surface, its speciation to pyridinic-N and the adequate active phase dispersion were essential to enhance the catalyst performance. On the other hand, activated carbon as catalyst support presented a high tolerance to ions other than NO_3^- present in the aqueous solution, showing a high stability during 100 h on stream.

CRediT authorship contribution statement

Conceptualization, A.F.M, E.D.; Methodology, I.S., E.D.; Investigation, I.S., E.D.; Writing – original draft, I.S., A.F.M, E.D.; Writing – review & editing, J.J.R., A.F.M, E.D.; Supervision, J.J.R., A.F.M, E.D.; Funding acquisition, A.F.M, E.D.

Funding

The authors greatly appreciate the financial support from the Spanish MICINN (PID 2019-108445RB-100), Comunidad de Madrid (S2018/EMT-4344). I. Sanchis wishes to thank the Comunidad de Madrid for PEJD-2017-PRE/AMB-4616 contract.

Declaration of Competing Interest

The authors declare that they have no known competing financial interests or personal relationships that could have appeared to influence the work reported in this paper.

Data Availability

Data will be made available on request.

Appendix A. Supporting information

Supplementary data associated with this article can be found in the online version at doi:10.1016/j.cattod.2023.01.018.

References

[1] H. Song, Y. Zhou, A. Li, S. Mueller, Selective removal of nitrate from water by a macroporous strong basic anion exchange resin, Desalination 296 (2012) 53–60, https://doi.org/10.1016/j.desal.2012.04.003.
[2] A.R.K. Gollakota, N. Kishore, S. Gu, A review on hydrothermal liquefaction of biomass, Renew. Sustain. Energy Rev. 81 (2018) 1378–1392, https://doi.org/10.1016/j.rser.2017.05.178.
[3] I. Mediavilla, R. Barro, E. Borjabad, D. Peña, M.J. Fernández, Quality of olive stone as a fuel: influence of oil content on combustion process, Renew. Energy 160 (2020) 374–384, https://doi.org/10.1016/j.renene.2020.07.001.
[4] B. Karpan, A.A.A. Ramana, M.K.T. Aroua, Waste-to-energy: coal-like refuse derived fuel from hazardous waste and biomass mixture, Process Saf. Environ. Prot. 149 (2021) 655–664, https://doi.org/10.1016/j.psep.2021.03.009.
[5] W.A.W. Mahari, E. Azwar, S.Y. Foong, A. Ahmed, W. Peng, M. Tabatabaei, M. Aghbashlo, Y.K. Park, C. Sonne, S.S. Lam, Valorization of municipal wastes using co-pyrolysis for green energy production, energy security, and environmental sustainability: a review, Chem. Eng. J. 421 (2021), 129749, https://doi.org/10.1016/j.cej.2021.129749.
[6] A. Jain, R. Balasubramanian, M.P. Srinivasan, Hydrothermal conversion of biomass waste to activated carbon with high porosity: a review, Chem. Eng. J. 283 (2016) 789–805, https://doi.org/10.1016/j.cej.2015.08.014.
[7] G. Ischia, L. Fiori, Hydrothermal carbonization of organic waste and biomass: a review on process, reactor, and plant modeling, Waste Biomass Valoriz. 12 (2021) 2797–2824, https://doi.org/10.1007/s12649-020-01255-3.
[8] M.H. Marzbali, S. Kundu, P. Halder, S. Patel, I.G. Hakeem, J. Paz-Ferreiro, S. Madapusi, A. Surapaneni, K. Shah, Wet organic waste treatment via hydrothermal processing: a critical review, Chemosphere 279 (2021), 130557, https://doi.org/10.1016/j.chemosphere.2021.130557.
[9] Z. Zhang, J. Yang, J. Qian, Y. Zhao, T. Wang, Y. Zhai, Biowaste hydrothermal carbonization for hydrochar valorization: skeleton structure, conversion pathways and clean biofuel applications, Bioresour. Technol. 324 (2021), 124686, https://doi.org/10.1016/j.biortech.2021.124686.

[10] A. Funke, F. Ziegler, Hydrothermal carbonization of biomass: a summary and discussion of chemical mechanisms for process engineering, Biofuels Bioprod. Bioref. 4 (2010) 160–177, https://doi.org/10.1002/bbb.198.
[11] E. Diaz, F.J. Manzano, J. Villamil, J.J. Rodriguez, A.F. Mohedano, Low-cost activated grape seed-derived hydrochar through hydrothermal carbonization and chemical activation for sulfamethoxazole adsorption, Appl. Sci. 9 (2019) 5127, https://doi.org/10.3390/app9235127.
[12] A. Sarrion, E. Diaz, M.A. de la Rubia, A.F. Mohedano, Fate of nutrients during hydrothermal treatment of food waste, Bioresour. Technol. 342 (2021), 125954, https://doi.org/10.1016/j.biortech.2021.125954.
[13] A. Álvarez-Murillo, E. Sabio, B. Ledesma, S. Román, C.M. González-García, Generation of biofuel from hydrothermal carbonization of cellulose. Kinetics modelling, Energy 94 (2016) 600–608, https://doi.org/10.1016/j.energy.2015.11.024.
[14] A. Jain, R. Balasubramanian, M.P. Srinivasan, Production of high surface area mesoporous activated carbons from waste biomass using hydrogen peroxide-mediated hydrothermal treatment for adsorption applications, Chem. Eng. J. 273 (2015) 622–629, https://doi.org/10.1016/j.cej.2015.03.111.
[15] M. Wilk, A. Magdziarz, I. Kalemba-Rec, M. Szymanska-Chargot, Upgrading of green waste into carbon-rich solid biofuel by hydrothermal carbonization: the effect of process parameters on hydrochar derived from acacia, Energy 202 (2020), 117717, https://doi.org/10.1016/j.energy.2020.117717.
[16] M. Volpe, L. Fiori, From olive waste to solid biofuel through hydrothermal carbonisation: the role of temperature and solid load on secondary char formation and hydrochar energy properties, J. Anal. Appl. Pyrolysis 24 (2017) 63–72, https://doi.org/10.1016/j.jaap.2017.02.022.
[17] C.W. Purnomo, D. Castello, L. Fiori, Granular activated carbon from grape seeds hydrothermal char, Appl. Sci. 8 (2018) 331, https://doi.org/10.3390/app8030331.
[18] G. Yang, S. Song, J. Li, Z. Tang, J. Ye, J. Yang, Preparation and CO_2 adsorption properties of porous carbon by hydrothermal carbonization of tree leaves, J. Mater. Sci. Technol. 35 (2019) 875–884, https://doi.org/10.1016/j.jmst.2018.11.019.
[19] S.B. Kabakcı, S.S. Baran, Hydrothermal carbonization of various lignocellulosics: fuel characteristics of hydrochars and surface characteristics of activated hydrochars, Waste Manag. 100 (2019) 259–268, https://doi.org/10.1016/j.wasman.2019.09.021.
[20] J. Li, P. Zhao, T. Li, M. Lei, W. Yan, S. Ge, Pyrolysis behavior of hydrochar from hydrothermal carbonization of pinewood sawdust, J. Anal. Appl. Pyrolysis 146 (2020), 104771, https://doi.org/10.1016/j.jaap.2020.104771.
[21] G. Zhu, L. Yang, Y. Gao, J. Xua, H. Chen, Y. Zhu, Y. Wang, C. Liao, C. Lu, C. Zhu, Characterization and pelletization of cotton stalk hydrochar from HTC and combustion kinetics of hydrochar pellets by TGA, Fuel 244 (2019) 479–491, https://doi.org/10.1016/j.fuel.2019.02.039.
[22] T.P. de Araújo, H.B. Quesada, R. Bergamasco, D.T. Vareschini, M.A.S.D. de Barrosa, Activated hydrochar produced from Brewer's spent grain and its application in the removal of acetaminophen, Bioresour. Technol. 310 (2020), 123399, https://doi.org/10.1016/j.biortech.2020.123399.
[23] L. Wang, Y. Chang, X. Zhang, F. Yang, Y. Li, X. Yang, S. Dong, Hydrothermal co-carbonization of sewage sludge and high concentration phenolic wastewater for production of solid biofuel with increased calorific value, J. Clean. Prod. 255 (2020), 120317, https://doi.org/10.1016/j.jclepro.2020.120317.
[24] L. Dai, B. Yang, H. Li, F. Tan, N. Zhu, Q. Zhu, M. He, Y. Ran, G. Hu, A synergistic combination of nutrient reclamation from manure and resultant hydrochar upgradation by acid-supported hydrothermal carbonization, Bioresour. Technol. 243 (2017) 860–866, https://doi.org/10.1016/j.biortech.2017.07.016.
[25] J.D. Marin-Batista, J.A. Villamil, S.V. Qaramaleki, C.J. Coronella, A.F. Mohedano, M.A. de la Rubia, Energy valorization of cow manure by hydrothermal carbonization and anaerobic digestion, Renew. Energy 160 (2020) 623–632, https://doi.org/10.1016/j.renene.2020.07.003.
[26] G. Saverettiar, D. Li, A. Gross, G. Ho, Hydrothermal carbonization of cattle paunch waste: process conditions and product characteristics, J. Environ. Chem. Eng. 8 (2020), 104487, https://doi.org/10.1016/j.jece.2020.104487.
[27] I. Idowu, L. Li, J.R.V. Flora, P.J. Pellechia, S.A. Darko, K.S. Ro, N.D. Berge, Hydrothermal carbonization of food waste for nutrient recovery and reuse, Waste Manag. 69 (2017) 480–491, https://doi.org/10.1016/j.wasman.2017.08.051.
[28] K. Akarsu, G. Duman, A. Yilmazer, T. Keskin, N. Azbar, J. Yanik, Sustainable valorization of food wastes into solid fuel by hydrothermal carbonization, Bioresour. Technol. 292 (2019), 121959, https://doi.org/10.1016/j.biortech.2019.121959.
[29] S. Venna, H.B. Sharma, P.H.P. Reddy, S. Chowdhury, B.K. Dubey, Landfill leachate as an alternative moisture source for hydrothermal carbonization of municipal solid wastes to solid biofuels, Bioresour. Technol. 320 (2021), 124410, https://doi.org/10.1016/j.biortech.2020.124410.
[30] R. Khoshbouy, F. Takahashi, K. Yoshikawa, Preparation of high surface area sludge-based activated hydrochar via hydrothermal carbonization and application in the removal of basic dye, Environ. Res. 175 (2019) 457–467, https://doi.org/10.1016/j.envres.2019.04.002.
[31] G.C. Becker, D. Wüst, H. Köhler, A. Lautenbach, A. Kruse, Novel approach of phosphate-reclamation as struvite from sewage sludge by utilising hydrothermal carbonization, J. Environ. Manag. 238 (2019) 119–125, https://doi.org/10.1016/j.jenvman.2019.02.121.
[32] J.A. Villamil, E. Diaz, M.A. de la Rubia, A.F. Mohedano, Potential use of waste activated sludge hydrothermally treated as a renewable fuel or activated carbon precursor, Molecules 25 (2020) 3534, https://doi.org/10.3390/molecules25153534.
[33] H.S. Kambo, A. Dutta, A comparative review of biochar and hydrochar in terms of production, physico-chemical properties and applications, Renew. Sustain. Energy Rev. 45 (2015) 359–378, https://doi.org/10.1016/j.rser.2015.01.050.
[34] J. Fang, L. Zhan, Y.S. Ok, B. Gao, Minireview of potential applications of hydrochar derived from hydrothermal carbonization of biomass, J. Ind. Eng. Chem. 57 (2018) 15–21, https://doi.org/10.1016/j.jiec.2017.08.026.
[35] M. Heidari, A. Dutta, B. Acharya, S. Mahmud, A review of the current knowledge and challenges of hydrothermal carbonization for biomass conversion, J. Energy Inst. 92 (2019) 1779–1799, https://doi.org/10.1016/j.joei.2018.12.003.
[36] M.A. Yahya, Z. Al-Qodah, C.W.Z. Ngah, Agricultural bio-waste materials as potential sustainable precursors used for activated carbon production: a review, Renew. Sustain. Energy Rev. 46 (2015) 218–235, https://doi.org/10.1016/j.rser.2015.02.051.
[37] J. Pallarés, A. González-Cencerrado, I. Arauzo, Production and characterization of activated carbon from barley straw by physical activation with carbon dioxide and steam, Biomass Bioenergy 115 (2018) 64–73, https://doi.org/10.1016/j.biombioe.2018.04.015.
[38] M. Mariana, A. Khalil H.P.S, E.M. Mistar, E.B. Yahya, T. Alfatah, M. Danish, M. Amayreh, Recent advances in activated carbon modification techniques for enhanced heavy metal adsorption, J. Water Process. Eng. 43 (2021), 102221, https://doi.org/10.1016/j.jwpe.2021.102221.
[39] M. Gayathiri, T. Pulingam, K.T. Lee, K. Sudesh, Activated carbon from biomass waste precursors: factors affecting production and adsorption mechanism, Chemosphere 294 (2022), 133764, https://doi.org/10.1016/j.chemosphere.2022.133764.
[40] J. Bedia, M. Peñas-Garzón, A. Gómez-Avilés, J.J. Rodriguez, C. Belver, A review on the synthesis and characterization of biomass-derived carbons for adsorption of emerging contaminants from water, J. Carbon Res. 4 (2018) 63, https://doi.org/10.3390/c4040063.
[41] K. MacDermid-Watts, E. Adewakun, T.D. Abhi, R. Pradhan, A. Dutta, Hydrothermal carbonization valorization as an alternative application for corn bio-ethanol by-products, J. Environ. Chem. Eng. 9 (2021), 105431, https://doi.org/10.1016/j.jece.2021.105431.
[42] B.R. Patra, A. Mukherjee, S. Nanda, A.K. Dalai, Biochar production, activation and adsorptive applications: a review, Environ. Chem. Lett. 19 (2021) 2237–2259, https://doi.org/10.1007/s10311-020-01165-9.
[43] N.A. Zubbri, A.R. Mohamed, P. Lahijani, M. Mohammadi, Low temperature CO_2 capture on biomass-derived KOH-activated hydrochar established through hydrothermal carbonization with water-soaking pre-treatment, J. Environ. Chem. Eng. 9 (2021), 105074, https://doi.org/10.1016/j.jece.2021.105074.
[44] W. Tu, Y. Liu, Z. Xie, M. Chen, L. Ma, G. Du, M. Zhu, A novel activation-hydrochar via hydrothermal carbonization and KOH activation of sewage sludge and coconut shell for biomass wastes: preparation, characterization and adsorption properties, J. Colloid Interface Sci. 593 (2021) 390–407, https://doi.org/10.1016/j.jcis.2021.02.133.
[45] Y. Gao, G. Hu, J. Zhong, Z. Shi, Y. Zhu, D.S. Su, J. Wang, X. Bao, D. Ma, Nitrogen-doped sp^2-hybridized carbon as a superior catalyst for selective oxidation, Angew. Chem. Int. Ed. 52 (2013) 2109–2113, https://doi.org/10.1002/anie.201207918.
[46] S.S. Shang, S. Gao, Heteroatom-enhanced metal-free catalytic performance of carbocatalysts for organic transformations, ChemCatChem 11 (2019) 3730–3744, https://doi.org/10.1002/cctc.201900336.
[47] Y. Wang, Z. Tang, S. Shen, J. Yang, The influence of heteroatom doping on the performance of carbon carbon-based electrocatalysts for oxygen evolution reactions, New Carbon Mater. 37 (2) (2022) 321–337, https://doi.org/10.1016/S1872-5805(22)60591-2.
[48] W.M. Chen, L. Qie, Y. Shen, Y.M. Sun, L.X. Yuan, X.L. Hu, W.X. Zhang, Y. H. Huang, Superior lithium storage performance in nanoscaled MnO promoted by N-doped carbon webs, Nano Energy 2 (2013) 412–418, https://doi.org/10.1016/j.nanoen.2012.11.010.
[49] K.H. Kim, S.J. Jeong, B.R. Koo, H.J. Ahn, Surface amending effect of N-doped carbon-embedded NiO films for multirole electrochromic energy-storage devices, Appl. Surf. Sci. 537 (2021), 147902, https://doi.org/10.1016/j.apsusc.2020.147902.
[50] D. Guo, Z. Li, P. Liu, M. Sun, N, P, S co-doped biomass-derived hierarchical porous carbon through simple phosphoric acid-assisted activation for high-performance electrochemical energy storage, Int. J. Hydrog. Energy 46 (2021) 8197–8209, https://doi.org/10.1016/j.ijhydene.2020.12.013.
[51] L. Roldan, Y. Marco, E. García-Bordeje, Bio-sourced mesoporous carbon doped with heteroatoms (N,S) synthesised using one-step hydrothermal process for water remediation, Microporous Mesoporous Mater. 222 (2016) 55–62, https://doi.org/10.1016/j.micromeso.2015.10.008.
[52] K. Huang, Z.L. Li, J.Y. Zhang, D.J. Tao, F. Liu, S. Dai, Simultaneous activation and N-doping of hydrothermal carbons by $NaNH_2$: an effective approach to CO_2 adsorbents, J. CO_2 Util. 33 (2019) 405–412, https://doi.org/10.1016/j.jcou.2019.07.012.
[53] E. Diaz, I. Sanchis, C.J. Coronella, A.F. Mohedano, Activated carbons from hydrothermal carbonization and chemical activation of olive stones: application in sulfamethoxazole adsorption, Resources 11 (2022) 43, https://doi.org/10.3390/resources11050043.
[54] X. Li, X. Huang, S. Xi, S. Miao, J. Ding, W. Cai, S. Liu, X. Yang, H. Yang, J. Gao, J. Wang, Y. Huang, T. Zhang, B. Liu, Single cobalt atoms anchored on porous n-doped graphene with dual reaction sites for efficient fenton-like catalysis, J. Am. Chem. Soc. 140 (2018) 12469–12475, https://doi.org/10.1021/jacs.8b05992.
[55] Z. Liu, X. Zhang, Z. Jiang, P. Yang, G. Gao, N-doped bamboo-like carbon nanotubes loading Co as ideal electrode material towards superior catalysis

performance, Int. J. Hydrog. Energy 45 (2020) 8703–8714, https://doi.org/10.1016/j.ijhydene.2020.01.153.

[56] Y. Shen, K. Zhu, D. He, J. Huang, H. He, L. Lei, W. Chen, Tetracycline removal via adsorption and metal-free catalysis with 3D macroscopic N-doped porous carbon nanosheets: non-radical mechanism and degradation pathway, J. Environ. Sci. 111 (2022) 351–366, https://doi.org/10.1016/j.jes.2021.04.014.

[57] Y.H. Li, T.H. Hung, C.W. Chen, A first-principles study of nitrogen- and boron-assisted platinum adsorption on carbon nanotubes, Carbon 47 (2009) 850–855, https://doi.org/10.1016/j.carbon.2008.11.048.

[58] A.B. Ayusheev, O.P. Taran, I.A. Seryak, O.Y. Podyacheva, C. Descorme, M. Besson, L.S. Kibis, A.I. Boronin, A.I. Romanenko, Z.R. Ismagilov, V. Parmon, Ruthenium nanoparticles supported on nitrogen-doped carbon nanofibers for the catalytic wet air oxidation of phenol, Appl. Catal. B 146 (2014) 177–185, https://doi.org/10.1016/j.apcatb.2013.03.017.

[59] J. Cai, S. Bennici, J. Shen, A. Auroux, The acid-base properties of nitrogen-containing mesoporous carbon materials, Microporous Mesoporous Mater. 212 (2015) 156–168, https://doi.org/10.1016/j.micromeso.2015.03.028.

[60] J.A. Baeza, N. Alonso-Morales, L. Calvo, F. Heras, J.J. Rodriguez, M.A. Gilarranz, Hydrodechlorination activity of catalysts based on nitrogen-doped carbons from low-density polyethylene, Carbon 87 (2015) 444–452, https://doi.org/10.1016/j.carbon.2015.02.068.

[61] F.T. You, G.W. Yu, Z.J. Xing, J. Li, S.Y. Xie, C.X. Lia, G. Wang, H.Y. Rena, Y. Wang, Enhancement of NO catalytic oxidation on activated carbon at room temperature by nitric acid hydrothermal treatment, Appl. Surf. Sci. 471 (2019) 633–644, https://doi.org/10.1016/j.apsusc.2018.12.066.

[62] G. Centi, S. Perathoner, Remediation of water contamination using catalytic technologies, Appl. Catal. B 41 (2003) 15–29, https://doi.org/10.1016/S0926-3373(02)00198-4.

[63] E.A. Davidson, M.B. David, J.N. Galloway, C.L. Goodale, R. Haeuber, J. A. Harrison, R.W. Howarth, D.B. Jaynes, R.R. Lowrance, B.T. Nolan, J.L. Peel, R. W. Pinder, E. Porter, C.S. Snyder, A.R. Townsend, M.H. Ward, Excess nitrogen in the U.S. environment: trends, risks, and solutions, Issues Ecol. 50 (2012).

[64] J. Martínez, A. Ortiz, I. Ortiz, State-of-the-art and perspectives of the catalytic and electrocatalytic reduction of aqueous nitrates, Appl. Catal. B 207 (2017) 42–59, https://doi.org/10.1016/j.apcatb.2017.02.016.

[65] G. Tokazhanov, E. Ramazanova, H. Shanawar, S. Bae, W. Lee, Advances in the catalytic reduction of nitrate by metallic catalysts for high efficiency and N_2 selectivity: a review, Chem. Eng. J. 384 (2020), 123252, https://doi.org/10.1016/j.cej.2019.123252.

[66] I. Sanchis, E. Diaz, A.H. Pizarro, J.J. Rodriguez, A.F. Mohedano, Nitrate reduction with bimetallic catalysts. A stability-addressed overview, Sep. Purif. Technol. 290 (2022), 120750, https://doi.org/10.1016/j.seppur.2022.120750.

[67] L.A. Deegan, A. Wright, S.G. Ayvazian, J.T. Finn, H. Golden, R.R. Merson, J. Harrison, Nitrogen loading alters seagrass ecosystem structure and support of higher trophic levels, Aquat. Conserv.: Mar. Freshw. Ecosyst. 12 (2002) 193–212, https://doi.org/10.1002/aqc.490.

[68] L.A. Deegan, Lessons learned: the effects of nutrient enrichment on the support of nekton by seagrass and salt marsh ecosystems, Estuaries 25 (2002) 727–742, https://doi.org/10.1007/BF02804902.

[69] J.M. Burkholder, D.A. Tomasko, B.W. Touchette, Seagrasses and eutrophication, J. Exp. Mar. Biol. Ecol. 350 (2007) 46–72, https://doi.org/10.1016/j.jembe.2007.06.024.

[70] J.M.C. Mesa, C.R. Armendáriz, A.H. de la Torre, Nitrate intake from drinking water on Tenerife island (Spain), Sci. Total Environ. 302 (2003) 85–92, https://doi.org/10.1016/S0048-9697(02)00341-8.

[71] N. Espejo-Herrera, K.P. Cantor, N. Malats, D.T. Silverman, A. Tardón, R. García-Closas, C. Serra, M. Kogevinas, C.M. Villanueva, Nitrate in drinking water and bladder cancer risk in Spain, Environ. Res. 137 (2015) 299–307, https://doi.org/10.1016/j.envres.2014.10.034.

[72] M.H. Ward, R.R. Jones, J.D. Brender, T.M. de Kok, P.J. Weyer, B.T. Nolan, C. M. Villanueva, S.G. van Breda, Drinking water nitrate and human health: an updated review, Int. J. Environ. Res. Public Health 15 (2018) 1557, https://doi.org/10.3390/ijerph15071557.

[73] Council Directive 91/676/EEC of 12 December 1991 concerning the protection of waters against pollution caused by nitrates from agricultural sources. ⟨http://data.europa.eu/eli/dir/1991/676/oj⟩.

[74] V.B. Jensen, J.L. Darby, C. Seidel, C. Gorman, Nitrate in potable water supplies: alternative management strategies, Crit. Rev. Environ. Sci. Technol. 44 (2014) 2203–2286, https://doi.org/10.1080/10643389.2013.828272.

[75] K.D. Vorlop, T. Tacke, Erste schritte auf dem weg zur edelmetallkatalysierten nitrat- und nitrit-entfernung aus trinkwasser, Chem. Ing. Tech. 61 (1989) 836–837, https://doi.org/10.1002/cite.330611023.

[76] L. Calvo, M.A. Gilarranz, J.A. Casas, A.F. Mohedano, J.J. Rodríguez, Denitrification of water with activated carbon-supported metallic catalysts, Ind. Eng. Chem. Res. 49 (2010) 5603–5609, https://doi.org/10.1021/ie100838r.

[77] A.H. Pizarro, C.B. Molina, J.J. Rodriguez, F. Epron, Catalytic reduction of nitrate and nitrite with mono- and bimetallic catalysts supported on pillared clays, J. Environ. Chem. Eng. 3 (2015) 2777–2785, https://doi.org/10.1016/j.jece.2015.09.026.

[78] A.H. Pizarro, I. Torija, V.M. Monsalvo, Enhancement of Pd-based catalysts for the removal of nitrite and nitrate from water, J. Water Supply Res. Technol. 67 (2018) 615–625, https://doi.org/10.2166/aqua.2018.024.

[79] F. Ruiz-Bevia, M.J. Fernandez-Torres, Effective catalytic removal of nitrates from drinking water: an unresolved problem? J. Clean. Prod. 217 (2019) 398–408, https://doi.org/10.1016/j.jclepro.2019.01.261.

[80] S. Hamid, S. Golagana, S. Han, G. Lee, M.R. Babaa, W. Lee, Stability of Sn-Pd-Kaolinite catalyst during heat treatment and nitrate reduction in continuous flow reaction, Chemosphere 241 (2020), 125115, https://doi.org/10.1016/j.chemosphere.2019.125115.

[81] I. Sanchis, E. Díaz, A.H. Pizarro, J.J. Rodríguez, A.F. Mohedano, Effect of water composition on catalytic reduction of nitrate, Sep. Purif. Technol. 255 (2021), 117766, https://doi.org/10.1016/j.seppur.2020.117766.

[82] I. Sanchis, J.J. Rodriguez, A.F. Mohedano, E. Diaz, Activity and stability of Pd bimetallic catalysts for catalytic nitrate reduction, Catalysts 12 (2022) 729, https://doi.org/10.3390/catal12070729.

[83] A.E. Palomares, C. Franch, A. Corma, Nitrates removal from polluted aquifers using (Sn or Cu)/Pd catalysts in a continuous reactor, Catal. Today 149 (3–4) (2010) 348–351, https://doi.org/10.1016/j.cattod.2009.05.013.

[84] J. Hirayama, Y. Kamiya, Tin-palladium supported on alumina as a highly active and selective catalyst for hydrogenation of nitrate in actual groundwater polluted with nitrate, Catal. Sci. Technol. 8 (19) (2018) 4985–4993, https://doi.org/10.1039/C8CY00730F.

[85] C. Franch, E. Rodríguez-Castellón, A. Reyes-Carmona, A.E. Palomares, Characterization of (Sn and Cu)/Pd catalysts for the nitrate reduction in natural water, Appl. Catal. A 425–426 (2012) 145–152, https://doi.org/10.1016/j.apcata.2012.03.015.

[86] A.E. Palomares, C. Franch, A. Corma, A study of different supports for the catalytic reduction of nitrates from natural water with a continuous reactor, Catal. Today 172 (2011) 90–94, https://doi.org/10.1016/j.cattod.2011.05.015.

[87] T. Yuranova, C. Franch, A.E. Palomares, E. Garcia-Bordejé, L. Kiwi-Minsker, Structured fibrous carbon-based catalysts for continuous nitrate removal from natural water, Appl. Catal. B 123–124 (2012) 221–228, https://doi.org/10.1016/j.apcatb.2012.04.007.

[88] M. Al Bahri, L. Calvo, M.A. Gilarranz, J.J. Rodriguez, F. Epron, Activated carbon supported metal catalysts for reduction of nitrate in water with high selectivity towards N_2, Appl. Catal. B 138–139 (2013) 141–148, https://doi.org/10.1016/j.apcatb.2013.02.048.

[89] Y. Yoshinaga, T. Akita, I. Mikami, T. Okuhara, Hydrogenation of nitrate in water to nitrogen over Pd–Cu supported on active carbon, J. Catal. 207 (2002) 37–45, https://doi.org/10.1006/jcat.2002.3529.

[90] K.G. Latham, W.M. Dose, J.A. Allen, S.W. Donne, Nitrogen doped heat treated and activated hydrothermal carbon: NEXAFS examination of the carbon surface at different temperatures, Carbon 128 (2018) 179–190, https://doi.org/10.1016/j.carbon.2017.11.072.

[91] A. Rey, J.A. Zazo, J.A. Casas, A. Bahamonde, J.J. Rodriguez, Influence of the structural and surface characteristics of activated carbon on the catalytic decomposition of hydrogen peroxide, Appl. Catal. A 402 (2011) 146–155, https://doi.org/10.1016/j.apcata.2011.05.040.

[92] A. Pintar, J. Batista, Catalytic hydrogenation of aqueous nitrate solutions in fixed-bed reactors, Catal. Today 53 (1999) 35–50, https://doi.org/10.1016/S0920-5861(99)00101-7.

[93] E. Muñoz, P. Marín, S. Ordóñez, F.V. Díez, The role of reaction kinetics and mass transfer in the selective catalytic reduction of NO with NH_3 in monolithic reactors, J. Chem. Technol. Biotechnol. 90 (2015) 1299–1307, https://doi.org/10.1002/jctb.4437.

[94] Y. Shao, H. Tan, D. Shen, Y. Zhou, Z. Jin, D. Zhou, W. Lu, Y. Long, Synthesis of improved hydrochar by microwave hydrothermal carbonization of green waste, Fuel 266 (2020), 117146, https://doi.org/10.1016/j.fuel.2020.117146.

[95] R.P. Ipiales, A.F. Mohedano, E. Diaz, M.A. de la Rubia, Energy recovery from garden and park waste by hydrothermal carbonisation and anaerobic digestion, Waste Manag. 140 (2022) 100–109, https://doi.org/10.1016/j.wasman.2022.01.003.

[96] A. Heredia-Moreno, R. Guillén-Bejarano, J. Fernández-Bolaños, M. Rivas-Moreno, Olive stones as a source of fermentable sugars, Biomass 14 (1987) 143–148, https://doi.org/10.1016/0144-4565(87)90016-3.

[97] G. Rodriguez, A. Lama, R. Rodriguez, A. Jimenez, R. Guillen, J. Fernandez-Bolaños, Olive stone an attractive source of bioactive and valuable compounds, Bioresour. Technol. 99 (2008) 5261–5269, https://doi.org/10.1016/j.biortech.2007.11.027.

[98] G.K. Parshetti, Z. Liu, A. Jain, M.P. Srinivasan, R. Balasubramanian, Hydrothermal carbonization of sewage sludge for energy production with coal, Fuel 111 (2013) 201–210, https://doi.org/10.1016/j.fuel.2013.04.052.

[99] K. Wiedner, C. Naisse, C. Rumpel, A. Pozzi, P. Wieczorek, B. Glaser, Chemical modification of biomass residues during hydrothermal carbonization – what makes the difference, temperature or feedstock, Org. Geochem. 54 (2013) 91–100, https://doi.org/10.1016/j.orggeochem.2012.10.006.

[100] A.E. Shalagina, Z.R. Ismagilov, O.Y. Podyacheva, R.I. Kvon, V.A. Ushakov, Synthesis of nitrogen-containing carbon nanofibers by catalytic decomposition of ethylene/ammonia mixture, Carbon 45 (2007) 1808–1820, https://doi.org/10.1016/j.carbon.2007.04.032.

[101] P. Treeweranuwat, P. Boonyoung, M. Chareonpanich, K. Nueangnoraj, Role of nitrogen on the porosity, surface, and electrochemical characteristics of activated carbon, ACS Omega 5 (2020) 1911–1918, https://doi.org/10.1021/acsomega.9b03586.

[102] J.L. Figueiredo, M.F.R. Pereira, M.M.A. Freitas, J.J.M. Orfao, Modification of the surface chemistry of activated carbons, Carbon 37 (1999) 1379–1389, https://doi.org/10.1016/S0008-6223(98)00333-9.

[103] C. Moreno-Castilla, M.V. Lopez-Ramon, F. Carrasco-Marin, Changes in surface chemistry of activated carbons by wet oxidation, Carbon 38 (2000) 1995–2001, https://doi.org/10.1016/S0008-6223(00)00048-8.

[104] X. Zhuang, H. Zhan, Y. Song, C. He, Y. Huang, X. Yin, C. Wu, Insights into the evolution of chemical structures in lignocellulose and non-lignocellulose biowastes during hydrothermal carbonization (HTC), Fuel 236 (2019) 960–974, https://doi.org/10.1016/j.fuel.2018.09.019.

[105] L. Zhao, L.Z. Fan, M.Q. Zhou, H. Guan, S. Qiao, M. Antonietti, M.M. Titirici, Nitrogen-containing hydrothermal carbons with superior performance in supercapacitors, Adv. Mater. 22 (2010) 5202–5206, https://doi.org/10.1002/adma.201002647.

[106] C. Vagner, G. Finqueneisel, T. Zimny, P. Burg, B. Grzyb, J. Machnikowski, J. V. Webe, Characterization of the surface properties of nitrogen-enriched carbons by inverse gas chromatography methods, Carbon 41 (2003) 2847–2853, https://doi.org/10.1016/S0008-6223(03)00412-3.

[107] S. Biniak, G. Szymanski, J. Siedlewski, A. Swiatkowski, The characterization of activated carbons with oxygen and nitrogen surface groups, Carbon 35 (1997) 1799–1810, https://doi.org/10.1016/S0008-6223(97)00096-1.

[108] L. Calvo, M.A. Gilarranz, J.A. Casas, A.F. Mohedano, J.J. Rodriguez, Effects of support surface composition on the activity and selectivity of Pd/C catalysts in aqueous-phase hydrodechlorination reactions, Ind. Eng. Chem. Res. 44 (2005) 6661–6667, https://doi.org/10.1021/ie0503040.

[109] G. de la Puente, J.J. Pis, J.A. Menendez, P. Grange, Thermal stability of oxygenated functions in activated carbons, J. Anal. Appl. Pyrolysis 43 (1997) 125–138, https://doi.org/10.1016/S0165-2370(97)00060-0.

[110] H. He, X. Xu, D. Liu, J. Li, Y. Wei, H. Tang, J. Li, X. Li, Z.Z. Xie, D. Qu, The impacts of nitrogen doping on the electrochemical hydrogen storage in a carbon, Int. J. Energy Res. 45 (2021) 9326–9339, https://doi.org/10.1002/er.6463.

[111] Y. Cao, S. Mao, M. Li, Y. Chen, Y. Wang, Metal/porous carbon composites for heterogeneous catalysis: old catalysts with improved performance promoted by N-doping, ACS Catal. 7 (2017) 8090–8112, https://doi.org/10.1021/acscatal.7b02335.

[112] M. Inagaki, M. Toyoda, Y. Soneda, T. Morishita, Nitrogen-doped carbon materials, Carbon 132 (2018) 104–140, https://doi.org/10.1016/j.carbon.2018.02.024.

[113] F. Gao, Y. Xue, P. Deng, X. Cheng, K. Yang, Removal of aqueous ammonium by biochars derived from agricultural residuals at different pyrolysis temperatures, Chem. Speciat. Bioavailab. 27 (2015) 92–97, https://doi.org/10.1080/09542299.2015.1087162.

[114] F.M. Zoppas, F.A. Marchesini, A. Devard, A.M. Bernardes, E.E. Miró, Controlled deposition of Pd and In on carbon fibers by sequential electroless plating for the catalytic reduction of nitrate in water, Catal. Commun. 78 (2016) 59–63, https://doi.org/10.1016/j.catcom.2016.02.012.

[115] E. Rahimi, G. Sajednia, M. Baghdadi, A. Karbassi, Catalytic chemical reduction of nitrate from simulated groundwater using hydrogen radical produced on the surface of palladium catalyst supported on the magnetic alumina nanoparticles, J. Environ. Chem. Eng. 6 (2018) 5249–5258, https://doi.org/10.1016/j.jece.2018.08.026.

[116] M. He, B. Xu, Q. Lu, Probing the role of surface speciation of tin oxide and tin catalysts on CO_2 electroreduction combining in situ Raman spectroscopy and reactivity investigations, Chin. J. Catal. 43 (2022) 1473–1477, https://doi.org/10.1016/S1872–2067(21)64014–7.

[117] A.O. Osikoya, D. Wankasi, R.M.K. Vala, C.W. Dikio, A.O. Afolabi, N. Ayawei, E. D. Dikio, Synthesis, characterization and sorption studies of nitrogen-doped carbon nanotubes, Dig. J. Nanomater. Biostruct. 10 (2015) 125–134.

[118] S. Hamid, M.A. Kumar, W. Lee, Highly reactive and selective Sn-Pd bimetallic catalyst supported by nanocrystalline ZSM-5 for aqueous nitrate reduction, Appl. Catal. B 187 (2016) 37–46, https://doi.org/10.1016/j.apcatb.2016.01.035.

[119] S. Hamid, S. Bae, W. Lee, Novel bimetallic catalyst supported by red mud for enhanced nitrate reduction, Chem. Eng. J. 348 (2018) 877–887, https://doi.org/10.1016/j.cej.2018.05.016.

[120] D. Liu, Y. Tong, X. Yan, J. Liang, S.X. Dou, Recent advances in carbon-based bifunctional oxygen catalysts for zinc-air batteries, Batter. Supercaps 2 (2019) 743–765, https://doi.org/10.1002/batt.201900052.

[121] V. Strelko Jr., D.J. Malik, M. Streat, Characterisation of the surface of oxidised carbon adsorbents, Carbon 40 (2002) 95–104, https://doi.org/10.1016/S0008-6223(01)00082-3.

[122] X. Yang, Y. Wan, Y. Zheng, F. He, Z. Yu, J. Huang, H. Wang, Y.S. Ok, Y. Jiang, B. Gao, Surface functional groups of carbon-based adsorbents and their roles in the removal of heavy metals from aqueous solutions: a critical review, Chem. Eng. J. 366 (2019) 608–621, https://doi.org/10.1016/j.cej.2019.02.119.

[123] B.P. Chaplin, E. Roundy, K.A. Guy, J.R. Shapley, C.J. Werth, Effects of natural water ions and humic acid on catalytic nitrate reduction kinetics using an alumina supported Pd-Cu catalyst, Environ. Sci. Technol. 40 (2006) 3075–3081, https://doi.org/10.1021/es0525298.

[124] Y. Wang, Y. Sakamoto, Y. Kamiya, Remediation of actual groundwater polluted with nitrate by the catalytic reduction over copper-palladium supported on active carbon, Appl. Catal. A 361 (1–2) (2009) 123–129, https://doi.org/10.1016/j.apcata.2009.04.006.